DEVELOPMENT OF THE OPTICAL FEEDBACK SYSTEM OF AN ATOMIC FORCE MICROSCOPE

By

Heidi M. Kroening

A thesis submitted in partial fulfillment of the requirements for the degree of

Bachelor of Science

Houghton College

February 2018

Signature of Author……………………………………………..……………………..
Department of Physics
February 17, 2018

……………………………………………………………………………………..
Dr. Brandon Hoffman
Associate Professor of Physics
Research Supervisor

……………………………………………………………………………………..
Dr. Kurt Aikens
Assistant Professor of Physics

DEVELOPMENT OF THE OPTICAL FEEDBACK SYSTEM OF AN ATOMIC FORCE MICROSCOPE

By

Heidi M. Kroening

Submitted to the Department of Physics
on February 17, 2018 in partial fulfillment of the
requirement for the degree of
Bachelor of Science

Abstract

A low-cost atomic force microscope (AFM) is under development at Houghton College. Once operating, the AFM will be used to characterize the surface topography of thin metal films, providing image resolution on the order of nanometers. The AFM will be equipped with a modified "Johnny Walker" sample mount to allow for a controlled approach of the sample to the cantilever tip. An optical laser system will be used to image the sample. The beam footprint of a laser reflected off a cantilever oscillating at its resonant frequency will be measured on a Conex PSD9 position sensing detector. A feedback loop written in LabVIEW will control the distance between the cantilever tip and the sample. In order to minimize vibrations, an eddy current and spring dampening system will be implemented.

Thesis Supervisor: Dr. Branson Hoffman
Title: Associate Professor of Physics

TABLE OF CONTENTS

TABLE OF FIGURES

Chapter 1

History and Motivation

1.1 Introduction

The development of the atomic force microscope (AFM) in the 1980s greatly advanced the field of scanning probe microscopy by introducing an atomic interaction between the sample and the scanning tip [1]. Similar to its predecessors, the scanning electron microscope and the scanning tunneling microscope, the AFM scans a sample surface to return a topographical image of the surface. On an AFM, the interaction between the tip and the sample creates an atomic force that is mapped as a high-resolution image of the surface topography, allowing the sample to be analyzed with nanometer resolution.

1.2 History

The knowledge that glass bends light and thus can be used to magnify an object has been around for over 2000 years. It is from this observation that lenses were created and used to craft glasses and magnifying lenses. In the 1590s, Hans and Zacharias Janssen invented the first optical microscope by placing lenses in a tube [2]. The optical microscope continued to evolve over the next 500 years allowing for the furthering of scientific exploration in fields requiring the use of magnification to collect data. However, due to the properties of refraction, the best of these microscopes only provide a maximum resolution of 0.2 μm, thus magnifying an object by 1500. While such microscopes were essential to understanding cells and tissues, as they could see much beyond that of the human eye, they lacked the ability to understand a structure on an atomic scale.

Out of this increased interest of studying samples at their molecular level came the development of the first electron microscope [3]. In 1931 Ernst Abbe Ruske and Max Knolle built a transmission electron microscope (TEM) [4]. Electrons are accelerated through a sample at a very high speed and are then focused on a screen to form a magnified image of the sample. Within the decade, a second electron microscope was developed, the scanning electron microscope (SEM) [4]. Instead of sending a high energy beam of electrons through a sample, a lower energy electron beam interacts with the sample surface, exciting atomic (or secondary) electrons in the sample. The intensity of the secondary electrons that exit the sample surface depends on the topography. An image is produced by scanning the beam along the sample surface. While an SEM can produce a sharper image than a TEM, it is not as powerful. For the next forty years the TEM and the SEM remained at the forefront of microscopy.

In 1981 Gerd Binnig and Heinrich Rohrer developed the scanning tunneling microscope (STM) [5]. This newest electron microscope earned them a Nobel Prize in Physics five years later. The STM introduced the use of a scanning probe. A voltage difference is applied to the metallic probe and the sample so that when the probe comes within angstroms of a sample, electrons pass from one to the other in a process called tunneling [6]. During the scanning process the probe is moved up and down to keep the tunneling current at a preset value. Thus, by tracking the probe's movement, the surface topography of the sample can be measured.

Not only was the STM able to provide greater resolution than ever before, but it did so while using lower energies than the high energy beams needed by the TEM and SEM. However, soon after the development of the STM Binnig began working on an idea that would use forces instead of a current to image a sample [5]. Together with Christoph Gerber and Calvin Quate they found that the key was creating a lever whose spring constant was weaker than the interaction force between the lever and the sample. They were confident that if the lever could deflect on the order of angstroms then this new invention would be able to take images on the atomic level.

In 1986, Binnig filed US Patent Claim #4724318 for the Atomic Force Microscope and Method for Imaging Surfaces with Atomic Resolution [7]. The design of the original AFM, included in the patent, is shown in Figure 1.

Binnig's AFM shared many components with his recently developed STM. A sample was made possible to move in directions x-y-z by a piezoelectric crystal. Then a spring-like cantilever with a sharp tip would approach the sample so closely that an interaction between the molecules in the tip and the sample would occur. This interaction would cause the cantilever to deflect and thus change the tunneling current across an STM tip. Using a feedback loop, the distance between the sample and the cantilever tip would change until the tunneling current returned to its preset value.

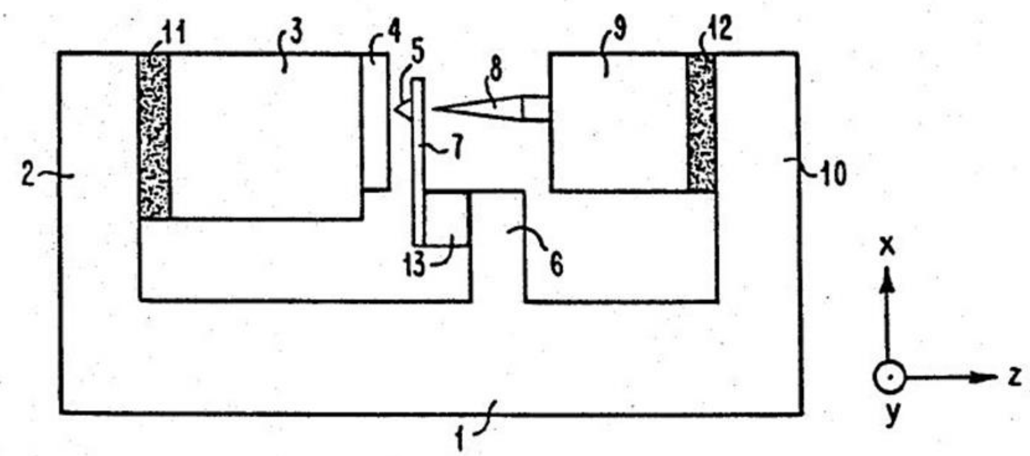

Figure 1. The AFM design published in the patent. A sharp point (5) is placed on a cantilever (7). A piezoelectric crystal (3) moves the sample (4) in directions x-y-z, allowing the tip to approach it. When scanning begins, the interaction between the atoms at the point and the surface of the sample force the cantilever to deflect. This creates a change in tunnel current which is monitored by a feedback loop. In order to regulate the current between the STM tip (8) and the cantilever the force between the sample and the tip changes by adjusting the distance between the two. Figure taken from Ref. [7].

Since its development in the 1980s the AFM has been a popular means of analysis [1,5,8,9]. Not only capable of providing higher resolution images than many of its predecessors, reaching resolution up to 10^{10} it does so without causing damage to the sample. The AFM is also applicable to both conductors and insulators because it does not use a current as the STM does. Still, changes have continued to be made to the original design to improve the AFM. One major change was replacing the STM component with an optical laser system. Instead of using the STM to detect the cantilever movement, a laser is reflected off the back of the cantilever into a position sensitive detector (PSD). Now the data from the detector is read into a feedback loop which will regulate the distance between the sample and the tip. This is the technique that the Houghton College AFM uses.

1.3 Motivation

One of the key areas of research in the Houghton College physics department is thin metal films. While thin films are not currently being developed at the college, the department's deposition chamber has shown that it has the ability to produce thin metal films. It is hoped that, with the production of these films, further study of them will be possible with the continued development of the department's other instruments including the AFM, an X-ray diffractometer (XRD), a scanning electron microscope (SEM), and a phase-stepping interferometer.

A thin film is a structure with one direction small compared to its extent in the other two directions [9]. The short distance between the two surfaces in a thin film influences the interaction between the surfaces and thus can affect the physical properties of the substance. When a film is made, the material's atoms create a crystal structure. Each sample has a different crystal structure and each structure has a different orientation in which it can present itself. Over time these orientations can change, thus making it important that the films are analyzed. Because of its high resolution output and since each orientation has a different surface structure, the AFM is able to detect the different crystalline structure orientations in a sample [10].

While the major motivation behind the development of the Houghton College AFM is the study of thin films, there is also an educational component to it. In order to avoid the price of a commercial AFM, which ranges from $26,000-$70,000 [11], a design for a low-cost AFM must be created. Implementing objects already found in a lab and purchasing only what cannot be made for less money, the construction of a low-cost AFM is possible. As students at Houghton College continue to construct an AFM that fits these criteria they develop important technological, communication, and problem solving skills.

The atomic force microscope continues to prove itself useful in the role of study and characterization of the surface topography of thin metal films [9,12]. If the deposition of a film is stopped before completion, an AFM can analyze the islands formed which may predict defects in the crystal structure. Upon completion, the films are analyzed and all atomic structural defects can be found. Building an atomic force microscope will not only enable Houghton College to join the current research on thin films and their surface topography, but will create an opportunity for the College to analyze their own thin metal films.

Chapter 2

THEORY

2.1 Introduction

Before construction on an AFM can begin there are important concepts that must be understood. Knowing the technical components needed is just the beginning. How the cantilever operates, what forces are introduced into the system, and how lenses work are all very important to the operation of the AFM. This chapter will briefly discuss the theory behind these topics, thus providing the necessary information to proceed.

2.2 Forces

AFM imaging relies on the atomic forces between the cantilever tip and the sample. The AFM allows for the measurement of forces that appear between surfaces that are separated by just fractions of microns [13]. The force diagram in Figure 2 shows the three forces on the oscillating cantilever while it is approaching the surface of the sample.

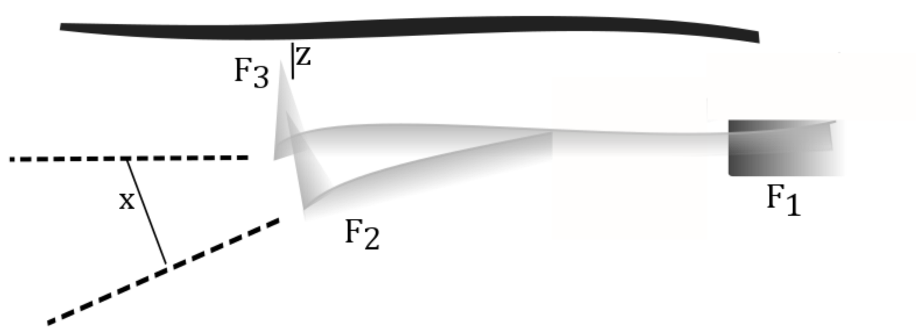

Figure 2. A force diagram of the oscillating cantilever as it approaches the sample. F_1 is the driving force of the cantilever holder, F_2 is the restoring force of the cantilever, and F_3 are the Van der Waals forces between the cantilever tip and the sample surface. The angle of cantilever deflection is represented by x and z is the distance between the relaxed cantilever and the sample. The positive direction is defined as the cantilever moves toward the sample.

The cantilever holder exerts a driving force, F_1, on the cantilever. A piezo element set in the holder oscillates the cantilever at its resonant frequency. The driving force produced by the holder is a sine wave with an amplitude, A, giving

$$F_1 = A \sin \omega_0 t. \tag{2.1}$$

F_2 is the restoring force of the cantilever which can be modeled as a harmonic oscillator;

$$F_2 = -kx. \tag{2.2}$$

The cantilever has a stiffness of k and a displacement of x. The restoring force can be written in terms of angular frequency, ω_0, where

$$\omega_0 = \sqrt{\frac{k}{m}} \tag{2.3}$$

and m is the mass of the cantilever. Since the angle of deflection of the cantilever is small, a small angle approximation can be applied with

$$x = \frac{z'}{L} \tag{2.4}$$

where z' is the distance that the end of the cantilever is from equilibrium and L is the length of the cantilever.

Substituting the angular frequency and small angle approximation in (2.2) gives

$$F_2 = \frac{-\omega_0^2\, m}{L}\, x. \tag{2.5}$$

The third force on the cantilever is an attractive Van der Waals (VdW) force, F_3. This force is introduced as the distance between the tip and the sample become small, on the order of angstroms. It is this force that causes the cantilever to deflect. Once this deflection is made constant, a constant force between tip and sample can be maintained.

To approximate this tip-sample force, the cantilever tip will be modeled as a sphere of radius R and the sample will be modeled as a flat surface as shown in Figure 3.

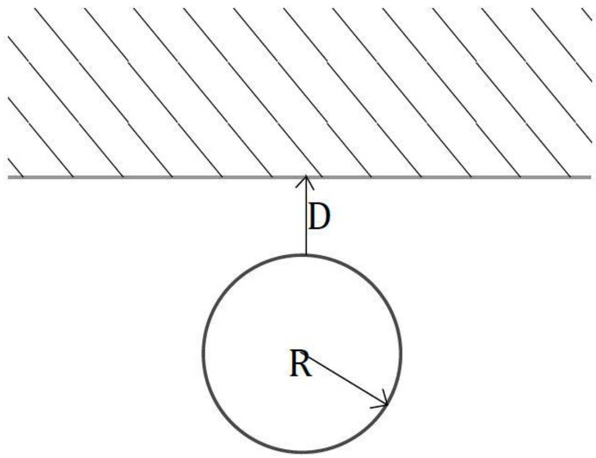

Figure 3. Model of the interaction between the cantilever tip and the surface. The tip has radius R and is mounted a small distance, D, below the surface.

The VdW potential between two molecules has the form $-\frac{C}{r^6}$ where C is the interatomic pair potential. This potential is then integrated over the volume of the tip and surface, where the separation of the two, D, is very small. This results in

$$W(D) = -\frac{BR}{6D}, D \ll R, \tag{2.6}$$

where $B = \pi^2 C\rho_1\rho_2$, is the Hamaker constant [14] with ρ_1, ρ_2 the number densities of the tip and the surface [15]. Taking the derivative of (2.5) will yield the VdW force needed to complete the force diagram,

$$F_3 = \frac{\pi C p_1 \rho_2 R}{6D^2}. \tag{2.7}$$

The total separation between the tip and the sample can be written as the sum of the distance between the relaxed tip and the sample and the distance the tip is from equilibrium,

$$D = z + z'. \tag{2.8}$$

A Taylor expansion about $z' = 0$ can be applied giving

$$F_3 = \frac{\pi C p_1 \rho_2 R}{6}\left(\frac{1}{z^2} - \frac{2z'}{z^3}\right). \tag{2.9}$$

The three forces acting on the cantilever can be summed to get

$$F_T = Asin(\omega_0 t) - \frac{(\omega_0^2 m)}{L} z' - \frac{\pi C \rho_1 \rho_2 R}{6}\left(\frac{1}{z^2} - \frac{2z'}{z^3}\right) = m\ddot{z}'. \tag{2.10}$$

This has a solution

$$z' = Z_0 \sin(\omega_0 t) + Z_1 \tag{2.11}$$

where the amplitude of oscillation, Z_0 can be written in terms of z

$$Z_0 = \frac{A}{\frac{\omega_o m}{L} - m\omega_0^2 - \frac{B}{3z^3}} \tag{2.12}$$

with a maximum at

$$z = \frac{B}{3\left(\frac{\omega_0 m}{L} - m\omega_0^2 - A\right)}^{\frac{1}{3}}. \tag{2.13}$$

Because a damping force is not taken into consideration here, Z_0 will have an infinite maximum. The addition of a damping force will phase shift (2.11) and provide a finite maximum for Z_0.

As the average tip-sample distance, z, changes, the force between tip and sample will change thus changing the amplitude of the cantilever's oscillations. Since the maximum amplitude of the cantilever tip occurs when the cantilever is driven at its resonant frequency, the resonant frequency is also dependent on tip-sample distance. The feedback system used to control the distance of the tip and the sample will be discussed in a following section.

2.3 Tip Movement

Binnig's original design of the AFM used a STM tip to track the tip movement of the cantilever as it scans the sample surface as seen in Figure 1. However, since the original design, an optical method has replaced the STM tip. The use of optics greatly reduces the force placed on the cantilever tip and is able to measure larger amplitude changes in the cantilever oscillations [16]. A laser beam is aimed at the aluminum-coating on the detector side of the cantilever and reflected into a detector. Based on the placement of the laser in the detector the movement of the cantilever can be analyzed. This movement has been derived in a previous paper [17]. It was shown that the larger the distance between the cantilever and the PSD, the higher the resolution will be.

2.4 Cantilever Operation

There are two main modes of operation with regard to scanning the sample within an AFM. It is important to know the difference between both modes, contact and tapping, in order to understand the difference their results may give. The Houghton College AFM implements a tapping mode cantilever.

2.4.1 Contact Mode

A cantilever operating in contact mode is moved across the surface of the sample. Using a feedback loop, the force on the cantilever tip is held constant, as it moves along the sample, and deflections of the cantilever are compared to a set value. A topological map of the sample surface can be created from the feedback loop. Although the easiest mode of operation to understand, it has some great disadvantages. Since a large force is pushing the cantilever against the sample, significant damage can occur to both the tip and the surface of the sample.

2.4.2 Tapping Mode

Operating in tapping mode provides a higher resolution and does not cause damage to the sample, as operating in contact mode does. The tip of the cantilever does not come in contact with the surface, which eliminates the frictional forces that create the damage to the surface when operated in contact mode. Instead, the cantilever is driven to vibrate near its resonance frequency. As the tip and the sample draw near, the forces between the two cause the amplitude of oscillations to change. The change is detected by the optical system. The walker will then move to adjust the distance between the sample and the cantilever until original amplitude is reached again. The optical system will continue to note the change in oscillation change and will plot the adjustments as they are made, thus giving a topographical map of the sample.

2.5 Piezoelectric Crystals

Certain crystalline materials have the ability to produce a charge when they are compressed. This concept is known as the piezoelectric effect. Similarly, when an electric potential is put across piezoelectric crystals, the atoms inside the crystal undergo pressure and become unbalanced. In an attempt to rebalance, the piezoelectric crystal will lengthen or contract in the direction of the applied electric field. This theory provides a way to control the movements needed for an AFM.

The ceramic tube shown in Figure 4 is a piezoelectric scanner tube. Four leads are attached to four outer quadrants of the tube and a fifth lead is attached inside. Two of the outer leads and the inner lead (1,3,5) are held at a constant voltage, c. The remaining leads (2,4) are set to scan in a saw tooth pattern between $0V$ and $2c$. As this force is exerted on the tubes, they slowly begin to bend. The tubes are then discharged allowing the tubes to straighten. The scanner tubes are mounted on sapphire balls which then sit on a polished surface. As the tubes straighten, the small coefficient of friction between the sapphire and the surface is overcome and the tube is able to slip minutely. Repeating this process gives the appearance that the device is walking on the surface.

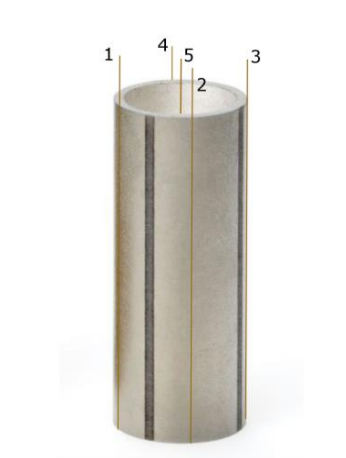

Figure 4. Image of a piezo scanner tube. Two opposing leads (1,3) and the inner lead (5) are set a constant voltage, c. The remaining two leads (2,4) scan between 0V and 2c. The force placed on the tube causes it to bend slowly. The charge is then quickly removed from the tube causing it to straighten. Figure edited from Ref [18].

The piezoelectric effect is also used to control the oscillations of the cantilever. As seen in Figure 5, a cantilever holder (Bruker DCHNM) houses a small piezoelectric element. A sine wave will be input to the element causing the cantilever, sitting above, to oscillate at its resonant frequency.

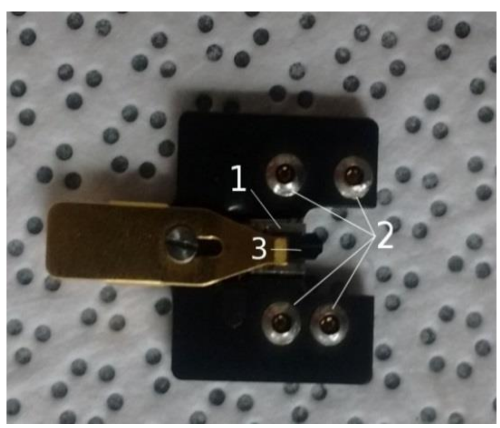

Figure 5. Image of the cantilever holder. The piezoelectric crystal (1) will be connected (2) to a program written in LabVIEW which will control the voltage being applied across it. The voltage will cause the piezo element to move which will in turn oscillate the cantilever (3) which is clamped directly above the piezoelectric crystal.

2.6 Lenses

In order to focus the laser on the cantilever and have it reflect into the PSD without compromising the intensity, a series of lenses are needed. Therefore, to utilize as much space as possible, a beam expander and a beam splitter are needed.

Lenses can be used to focus or disperse a beam of light. While only a converging lens is used directly in the AFM setup, a diverging lens is implemented in the beam expander.

2.6.1 Converging and Diverging Lens

Introducing lenses into the optical system allows for the manipulation of the path that the laser beam will take. Instead of having the beam travel straight from the source to the cantilever tip to the detector, lenses can bend the beam around obstacles and help in focusing the beam spot.

A converging lens bends the passing light rays toward each other along the lens' principle axis. In contrast the light rays passing through a diverging lens bend away from each other. For both converging and diverging lenses, any ray that enters one side of the lens parallel to the principle axis will converge or diverge, respectively, from the focal point, F, on the other side of the lens as shown in Figure 6. A converging lens has a positive focal length, f, while a diverging lens has a negative focal length.

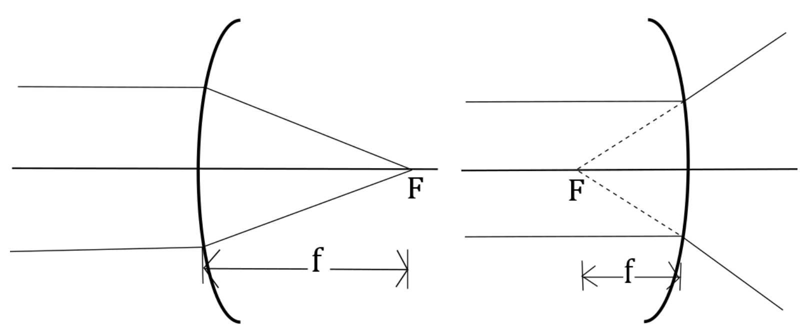

Figure 6. A drawing of a converging and a diverging thin lens. The image on the left shows a collimated beam converging to the focal point of the lens, F. The image on the right shows the collimated beam diverging after passing through the lens.

It follows from the ray diagram of a simple lens, shown in Figure 7, that the Gaussian lens equation for both a positive and negative thin lens is

$$\frac{1}{f} = \frac{1}{d_o} + \frac{1}{d_i}. \tag{2.14}$$

where d_o is the object distance and d_i is the image distance.

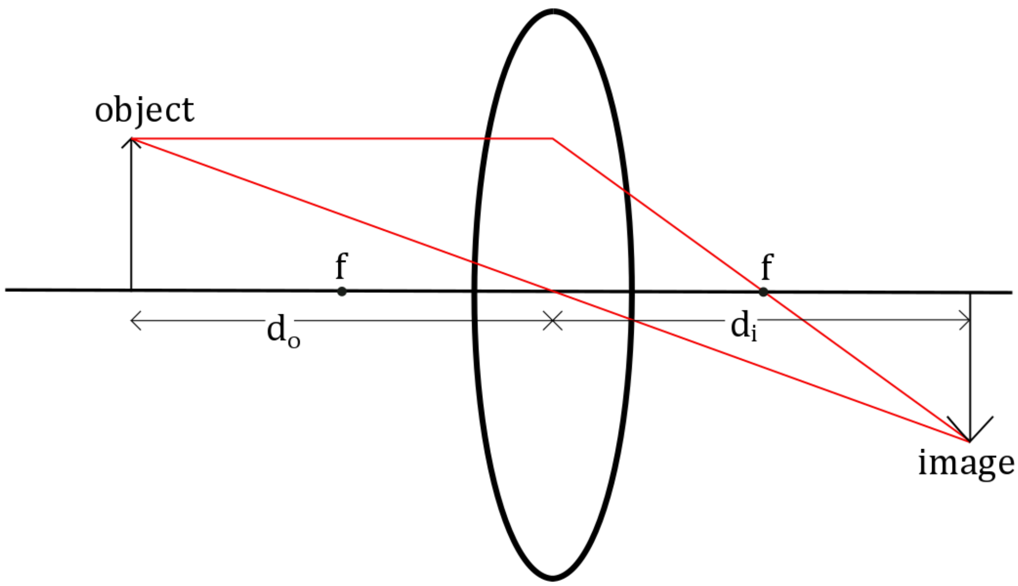

Figure 7. Illustration of a simple lens ray diagram. A ray diagram provides a convenient way to trace the light path. Knowing two of the following: object distance, d_o, image distance, d_i, or focal point of the lens allows for the third unknown to be found.

The Houghton AFM implements thick lenses, meaning the thickness of the lens must be taken into account unlike that of a thin lens. Figure 8 shows the geometry of a thick lens.

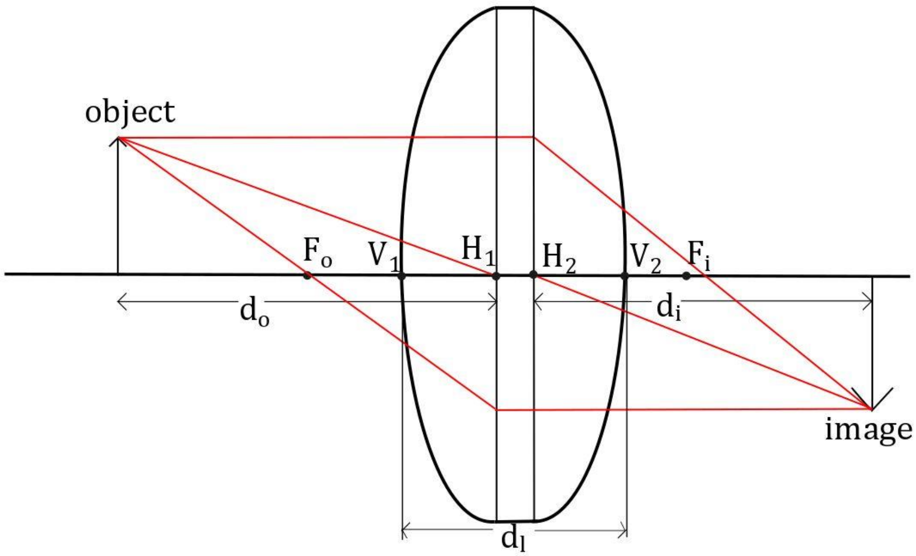

Figure 8. Drawing of thick-lens geometry. The thickness of lens, d_l, is measured by $\overline{V_1V_2}$. The object and image foci, F_0 and F_i are measured as their respective distances from $V_1$and V_2.The point H_1 lies along the primary principal plane while H_2 lies on the secondary principal plane.

A thick lens can be thought of as a combination of simple lenses and thus has two focal points. The first focal point is an object point on the primary axis of the lens which is imaged as the lens goes to infinity. The second focal point is an image point on the primary axis made from an object infinitely far away. When the diverging rays from the first focal point intersect, they lie in the primary principal plane. Similarly, the rays from the second focal point can be drawn back to the lens to find their intersect in the second principal plane.

A thick lens is modeled as two refracting, spherical surfaces with a distance d_l between them. Therefore, the relationship between object distance, image distance, and focal length remains the same as for a thin lens and the Gaussian lens equation of (2.14) can be applied to thick lenses. However, the focal length can also be found in terms of radius of curvature, R_j, and index of refraction, n_j,

$$\frac{1}{f} = (n_l - 1)\left[\frac{1}{R_1} - \frac{1}{R_2} + \frac{(n_l - 1)d_l}{n_l R_1 R_2}\right]. \tag{2.15}$$

The above equation provides information for a thick lens focal length, but it is only the first step in explaining the ray path through the lens. For this, ray tracing is introduced, illustrated in Figure 9.

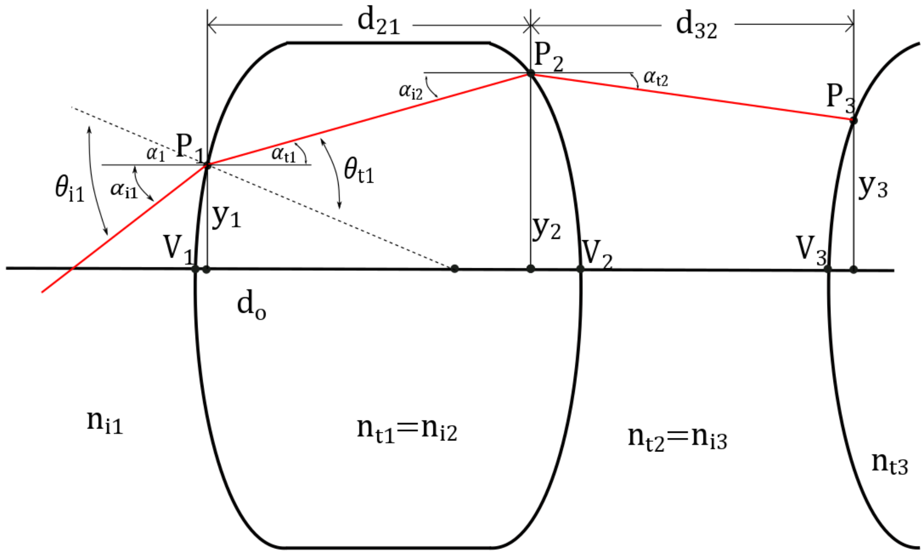

Figure 9. Thick lens ray tracing diagram. As the ray is traced through the lens, a serious of incident and transfer angles are created. The ray undergoes refraction at P_1then caries through the lens to P_2. The refraction and transfer equations are created from this process to represent the path of the ray.

To analyze the ray diagram a small angle approximation can be used to assume a flat surface. Starting with Snell's Laws

$$n_1\theta_1 = n_2\theta_2 \tag{2.16}$$

and applying to P_1 in Figure 9 gives

$$n_{ij}(\alpha_{ij} + \alpha_j) = n_{tj}(\alpha_{tj} + \alpha_j) \tag{2.17}$$

where α_{ij} is the angle between the principle axis and the ray incident on the j^{th} surface, α_{tj} is the angle between the principle axis and the ray transmitted from the j^{th} surface, and α_j is the angle between the principle axis and the normal.

Because $\alpha_j = \frac{y_j}{R_j}$, where y_j is the height of P_j, it follows

$$n_{ij}\left(\alpha_{ij} + \frac{y_j}{R_j}\right) = n_{tj}\left(\alpha_{tj} + \frac{y_j}{R_j}\right). \tag{2.18}$$

This can be rearranged to yield the refraction equation

$$n_{tj}\alpha_{tj} = n_{ij}\alpha_{ij} + \left(\frac{n_{ij} - n_{tj}}{R_j}\right) y_i. \tag{2.19}$$

Since

$$\frac{1}{f_j} = \frac{n_{ij} - n_{tj}}{R_j} \tag{2.20}$$

the ray angles have been in terms of focal length. After the ray refracts at P_1 it passes through the lens to P_2. This height is expressed as the transfer equation

$$y_{(j+1)} = y_j + d_{(j+1)j}\alpha_{tj}. \tag{2.21}$$

Together, equations (2.19) and (2.21) can be used to trace a ray through an entire lens system. A matrix method has been developed to simplify the process of thick lens analysis. Matrix analysis multiplies a series of refraction and transmission matrices together in order to appropriately trace the ray through the desired system. Setting (2.19) and (2.21) in matrix form develops two systems of equations. The refraction matrix

$$\begin{bmatrix} n_{tj}\alpha_{tj} \\ y_{tj} \end{bmatrix} = \begin{bmatrix} 1 & -\frac{n_{tj} - n_{ij}}{R_j} \\ 0 & 1 \end{bmatrix} \begin{bmatrix} n_{ij}\alpha_{ij} \\ y_{ij} \end{bmatrix} \tag{2.22}$$

transforms the rays $\overrightarrow{r_{ij}}$ into the ray $\overrightarrow{r_{tj}}$ which can be written as

$$\overrightarrow{r_{tj}} = \mathcal{R}_j \overrightarrow{r_{ij}}. \tag{2.23}$$

Similarly the transfer matrix

$$\begin{bmatrix} n_{i(j+1)}\alpha_{i(j+1)} \\ y_{(j+1)} \end{bmatrix} = \begin{bmatrix} 1 & 0 \\ \frac{d_{(j+1)j}}{n_{tj}} & 1 \end{bmatrix} \begin{bmatrix} n_{tj}\alpha_{tj} \\ y_j \end{bmatrix} \tag{2.24}$$

takes the transmitted ray $\overrightarrow{r_{tj}}$ and transforms it into the incident ray $\overrightarrow{r_{i(j+1)}}$, or

$$\overrightarrow{r_{i(j+1)}} = \mathcal{T}_j \overrightarrow{r_{tj}}. \tag{2.25}$$

Ultimately the angle of deflection of the reflected beam due to the bending of the cantilever is desired, and this can be found by monitoring the movement of the beam on the PSD. This final angle can be found by tracing the beam from the beginning of the system to the end. A system matrix, $\mathcal{A}$, is created by multiplying the series of transfer and refraction matrices needed to carry the ray through the system.

2.7 Beam Waist

The waist of a beam is where the beam width is at its smallest. This point will also be where the beam's intensity is at its largest. Since the angle of deflection of the laser off the cantilever can be measured by noting how far the beam moves on the PSD, the size of the beam hitting the PSD must be taken into account.

Before the outgoing beam from the laser can reach the PSD, it will pass through a series of lenses. The final lens in the system, $L2$ in Figure 10, will be used to adjust the beam width to allow it to hit the PSD as focused as possible. The beam will have two waists, before it enters the lens and after. Figure 10 illustrates the beam waists before and after the beam enters a converging lens. The incoming beam has waist w_1 a distance u from the lens; the outgoing beam has waist w_2 a distance v from the lens.

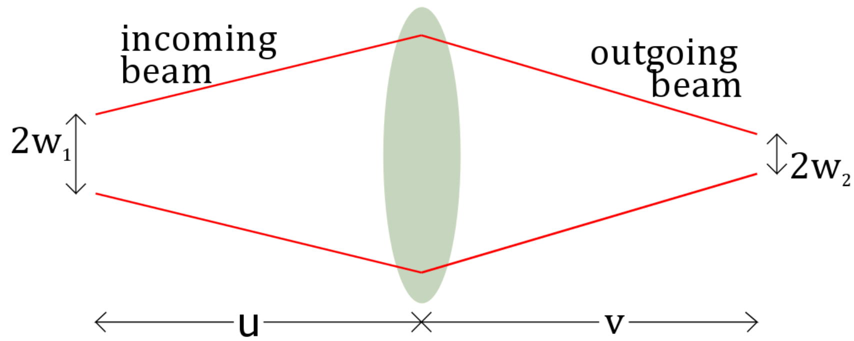

Figure 10. Illustration of the incoming and outgoing beam waists. The distance between the incoming beam and the lens is u while the distance between the lens and the outgoing beam is v.

The radius of beam I, $r_i\ (z)$, can be found in terms of the beam waist, w_i, where z is the distance between the two. It has been shown [19] that this relationship can be described as

$$r_i(z) = w_i\sqrt{1 + \frac{z^2\lambda^2}{\pi^2 w_i^4}}, \tag{2.26}$$

where λ is the wavelength of the incoming beam.

As $\frac{z}{w_i} \to \infty$, it is noted that the function, $r_i(z) \to \frac{z\lambda}{\pi w_i}$. Therefore, as the beam passes through a converging lens, the beam radius at the lens can be written in terms of the waist of the incoming and outgoing beams

$$w \approx \frac{u\lambda}{\pi w_1} \text{ and } w \approx \frac{v\lambda}{\pi w_2}. \tag{2.27}$$

Setting the beam radius equal and solving for a ration of the waists provides

$$\frac{w_2}{w_1} \approx \frac{v}{u}. \tag{2.28}$$

Thus the outgoing distance must be shorter than the incoming distance in order for the outgoing waist to be smaller. However, because some distance v must exist due to the mechanics of the system, u

must be made large. By introducing a large-diameter beam, it is mechanically easier to achiever a large u. Therefore, the incoming beam should be a large-diameter collimated beam so that it can pass through a converging lens to provide a minimized and focused beam spot on the PSD.

Chapter 3

Apparatus

3.1 Houghton AFM

An overall design for the Houghton College AFM was first created in 2008 [20]. While many changes have been made to individual components since, the general design remains much the same. A basic design of the AFM is shown in Figure 11. Current work on the AFM is focused on designing and testing the optical components and the "Johnny Walker" device. As such, the overall design has yet to be tested.

There are two major components to the AFM, the "Johnny Walker" device (3-6 in Figure 11) and the cantilever (7) and its optical system (8-9). Both of these components are supported by a vibration isolation stage (1). The stage is fitted with eddy-current dampers and supported by four springs (2). This system helps to eliminate the vibrations of the environment to allow for more accurate measuring.

The "Johnny Walker" device consists of three piezoelectrics and the sample mount, each attached to a plastic disk. This disk will be placed on the isolation stage and "walk" the sample to the cantilever. The cantilever will be placed underneath the sample mount on the under-side of the isolation stage. A laser will be sent through a series of optical devices to reflect off the cantilever and into a position sensing detector (PSD) which will record the beam footprint. In order to keep the cantilever oscillations constant a feedback loop is introduced. As the beam footprint is measured, the feedback circuit will determine how the cantilever needs to move, by way of the cantilever holder, in order to keep the cantilever at its resonant frequency.

The vibration parameters of the laser footprint on the PSD will be read into a program written in LabVIEW. Here the oscillation parameters of the laser footprint will be compared to the signal driving the cantilever. The output will be read into another LabVIEW program which will decide what change needs to happen to keep average tip-sample distance constant. This program will control the piezoelectrics in the walker and the cantilever. If necessary, a signal will be sent to the walker telling it to move closer to or father away from the cantilever. The computer is then able to give an image of the x-y position of the walker and the beam movement on the PSD.

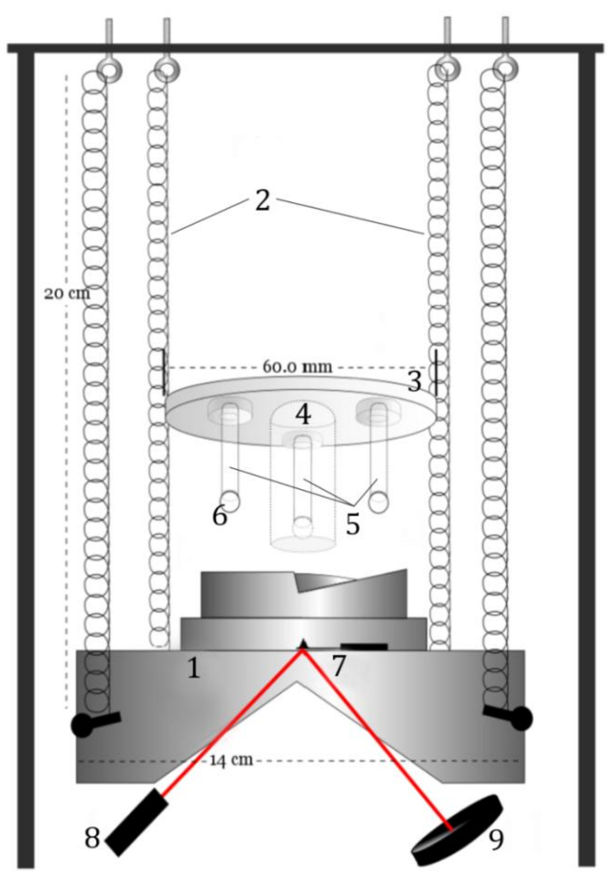

Figure 11. Schematic of the Houghton College atomic force microscope. An isolation stage (1) is supported by springs (2). A small acrylic disk (3) holds the sample mount (4) and three piezoelectric crystals (5). The piezoelectrics are mounted on sapphire balls (6) to allow for the sample to "walk" up and down the ramp to meet the vibrating cantilever (7). A laser (8) is directed at the cantilever and reflects into the position sensing detector (9). Figure edited from Ref. [21].

3.2 "Johnny Walker" Design

To control the movement of the sample as it approaches the oscillating cantilever, a "Johnny Walker" device was created [21] (see Figure 12). The device consists of a plastic disk (1) on which three piezoelectric tubes (2) are attached. Each tube has a sapphire ball glued to its base to allow it to "walk" up and down the ramp. A ceramic leg is attached to the center of the disk on which the sample is mounted (not placed yet).

The circular disk is made of acrylic and is 58 mm in diameter and 2.8 mm thick. The three piezoelectric tubes were epoxied into three holes equidistant from the center of the mount. Four wires (3) were connected to the leads on the outside of each tube and one on the inside of each using a conductive epoxy. The leads each carry a set voltage which is applied across the tubes. The voltage is applied slowly so that the tubes bend but do not slip on the surface. The tubes are then discharged allowing the tubes to straighten. As they straighten the small coefficient of friction between the sapphire and the ramp will be overcome and the walker should be able to slip a distance of several micrometers. Repeating this process will give the appearance that the device is walking up and down the ramp. Such fine movement of the walker enables the user to control where the sample comes in contact with the cantilever.

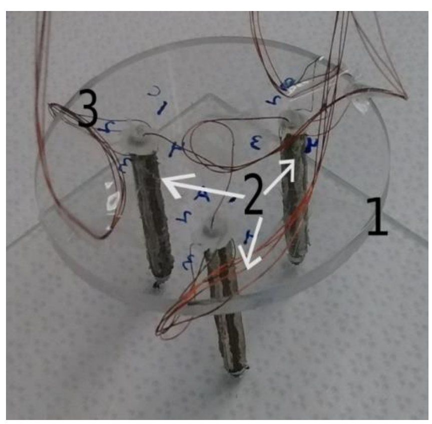

Figure 12. Figure of the current walker design. Three holes were drilled into the acrylic base (1) to form an equilateral triangle. Three piezoelectric tube scanners (2) were epoxied into the holes. Five wires were clued to each of the tubes.

3.3 Stage

3.3.1 Isolation Stagee

The isolation stage in Figure 13 is designed to support both the walker and the optical system. The isolation stage is made of aluminum and suspended by four springs from a solid aluminum frame which in turn is secured to an optical table. As the isolation stage moves with relation to the frame, the springs provide a restorative force to the entire system. To reduce mechanical oscillations from the entire system an eddy current dampening system is used. Four magnets are rigidly attached to the frame. They are positioned within slots in the isolation stage such that they move in and out of the slots as the stage oscillates. As the stage moves, it induces a current to oppose the change in magnetic flux it experiences. The induced current produces a magnetic force that opposes the motion of the stage.

When the existing stage was originally designed in 2008, little progress had been made on the optical system. As the optics have been modified they have also expanded beyond the holding capacity of the stage. In order to accommodate for the growing designs a new stage will have to constructed. The stage will still be built with a dampening system and with the ability to mount the ramp, explained in the next section, but will need to hold the weight of the optical system and not add obstruction to the beam path.

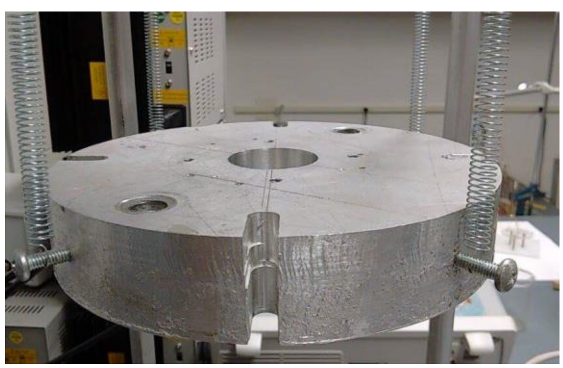

Figure 13. A photograph of the isolation stage. The isolation stage is suspended from four springs which are secured to an optical table. Magnets mounted on the frame will be positioned within the slots on the side of the stage in order to create an eddy current dampening system.

3.3.2 The Ramp

Sitting on top of the isolation stage is the ramp (Figure 14) on which the Johnny Walker is placed. The ramp is cut into three smaller ramps, each angled at 10° above the horizontal. The ramp is made from aluminum and has been polished to provide an appropriate surface for the walker to move on. It is mounted on a larger aluminum disk which is then screwed onto the isolation stage. The cantilever holder (see Figure 5) will be placed in the small crevice made between the larger disk and the ramp so that the cantilever tip points up toward the sample on the walker.

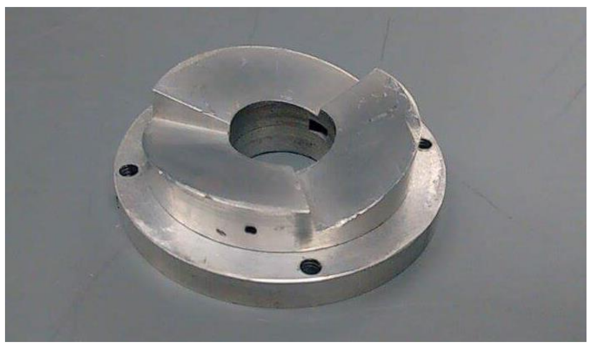

Figure 14. Photograph of the ramp fitted on the larger aluminum disk. The walker will move up and down the surface of the ramp to approach the cantilever. The cantilever will be placed inside the crevice such that the tip sticks up through the center hole.

3.4 Optics

The sample mount will approach the oscillating cantilever as the "Johnny Walker" device moves up and moves down the ramp, allowing the cantilever to begin collecting data. In order to collect and record this data, an optical system is being designed.

3.4.1 Original Design

The original design of the AFM's optical system included a laser and a quadrant detector. The laser reflected off the back of the oscillating cantilever into the quadrant detector [20]. The quadrant detector was then connected to a computer that was running a program written in LabVIEW. This program was designed to analyze the data the detector was collecting from the movement of the cantilever. However, due to the internal programming of the detector it did not run effectively in LabVIEW. Because using the LabVIEW environment to read the data had shown itself straightforward, it was decided to purchase a new detector that would be compatible with the system.

3.4.2 Current Design

The current detector is a tetra-lateral position sensing detector, a Conex-PSD9, designed to be compatible with LabVIEW software. The tetra-lateral PSD records linear XY positioning of the laser beam over the entire 9x9 mm sensor while also providing a signal proportional to the power of the laser beam.

The tetra-lateral effect diode of the PSD allows for the power of the laser beam to be monitored. The Conex-PSD9 can map the position of a laser with wavelength within 320-1100 nm and has a recommended power range of 10-80% of the maximum power [22] as shown in Figure 15. The original laser being used had maximum power 0.5 mW and wavelength 650 nm, but after reflecting off the cantilever tip the PSD was only able to read about 7% of the laser's total power.

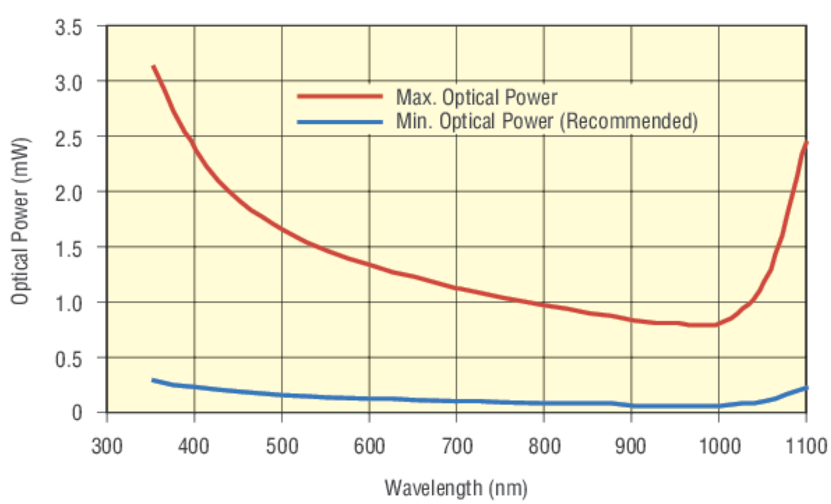

Figure 15. Graph of the position sensing detectors optical power as a function of wavelength. The red line shows the maximum optical power in milliwatts vs wavelength in nanometers while the blue line shows the recommended minimum optical power vs wavelength. Figure taken from Ref [22].

The Houghton College AFM now uses a LDM150 laser in the optical setup. Not only does the LDM150 provide the necessary power to make useful readings, it has an adjustable lens for ease of focus. The laser has a wavelength of 655 nm and a power of 3 mW. The increased intensity of the LDM150 permits for a filter to be placed in front of the PSD to adjust the amount of light entering the detector as needed.

The aluminum coating on the back of the cantilever provides a reflective surface for the laser beam. A converging lens is mounted on the laser producing a focal length of 1.5 mm. The laser is placed 17.5 mm away from the cantilever so that the beam will hit the 30 μm wide cantilever. To optimize the size of the beam spot on both the cantilever and the PSD, a series of optical lenses is placed between the laser and the cantilever as seen in Figure 16.

The intensity of the laser is largest where the beam width is smallest. This means the outgoing waist of the beam needs to be smaller than the incoming waist. Thus to achieve a small beam footprint, a collimated beam is focused onto the cantilever using a small-focus converging lens. In order for this spot to land on the PSD, the distance between the PSD and the cantilever needs to be minimized as the distance between the laser and the cantilever is increased. A beam splitter is added to the system to create a large-diameter collimated beam therefore requiring the distance between laser and cantilever to increase.

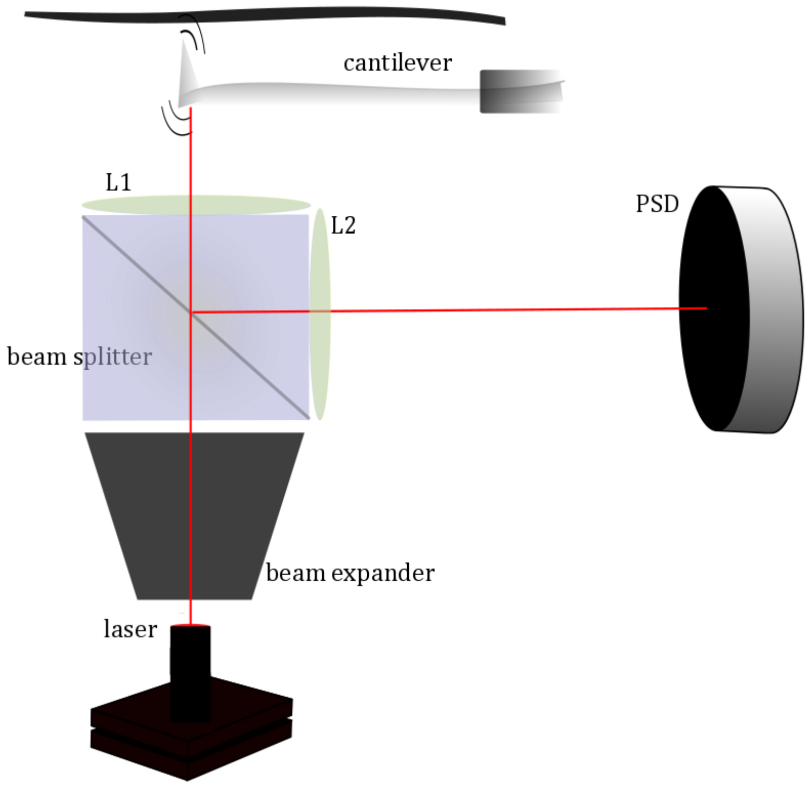

Figure 16. Illustration of the proposed completed optical system. The laser is centered in an optical positioner where it is directed through a series of lenses. As the beam enters the beam expander, it diverges and is then collimated. It then passes through a beam splitter and to a converging lens, $L1$. $L1$ converges the beam to a small focused point on the cantilever tip. The beam reflects off the tip and is diverging as it enters $L1$. $L1$ collimates the beam as it passes the beam splitter. The percentage of the light being recorded is sent horizontally through the beam splitter where it passes through another converging lens, $L2$. $L2$ has a long focal point creating a high resolution beam spot on the PSD.

A major issue in the original setup was space constraints. The design first consisted of the laser in its optical positioner and the cantilever holder as seen in Figure 17. This simplistic design would have provided for an easy mounting onto the stage. However, the setup was not able to focus the beam on the cantilever and reflect a spot into the PSD. Therefore a beam splitter is placed between the laser and the cantilever tip so that the return beam can reflect into the PSD without being blocked by any other piece of mechanics.

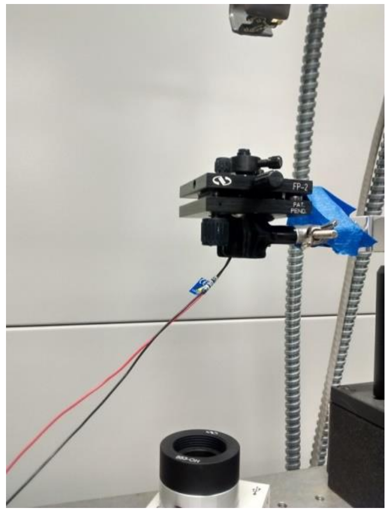

Figure 17. Picture of original optical setup. With the laser (middle) placed in the optical positioner, the beam was unable to focus on the cantilever (top) and reflect into the PSD (bottom).

The laser is placed in an optical positioner, a Newport FP-2A, shown in Figure 18. The two leads from the laser run through the center of the positioner and are connected to a power supply. With five degrees of freedom, XYZ$\Theta_x\Theta_y$. on the positioner, the user is able to make minor adjustments (on the order of micrometers) to the position of the laser so the beam spot hits the cantilever tip without any obstructions.

Figure 18. Figure of the laser optical positioner. The laser is placed in the center of the positioner with its leads accessible through the bottom of the positioner. The positioner can be adjusted in XYZ$\Theta_x\Theta_{y.}$.

The laser is then sent through a beam expander, Figure 19, into a beam splitter, through a converging lens, $L1$, and is then reflected off the cantilever tip. The beam expander creates a large-diameter collimated beam and $L1$ will have a short focal length in order to produce a small beam spot on the cantilever.

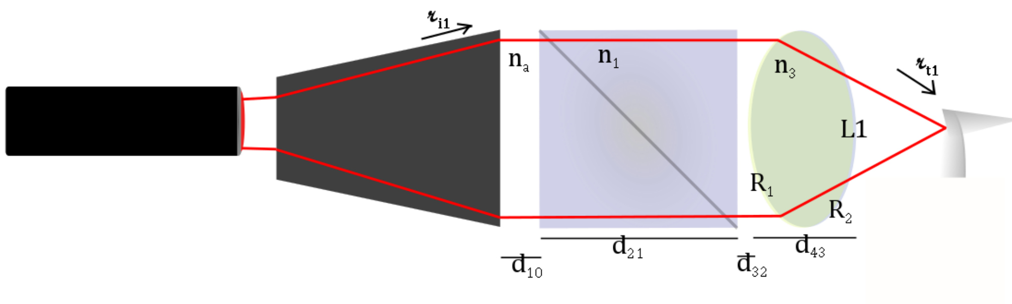

Figure 19. Drawing of the optics from the laser to the cantilever. The beam travels left to right. The beam expander diverges the beam then collimates it to make a large-diameter collimated beam. This beam passes through the beam splitter to the converging lens. The converging lens has a short focal point and will make a small focused beam spot on the cantilever.

In the setup shown above, the laser, beam splitter, and cantilever have already been determined. The beam expander will be determined on the maximum diameter size of beam able to fit in the splitter, and the focal length of $L2$ will be chosen after matrix ray analysis. To create the $\mathcal{A}$ matrix for the path from laser to cantilever the ray is transmitted from the beam expander to the beam splitter, through the beam splitter, and then from the beam splitter to the lens. It is then refracted through the left surface of the lens, transmitted through the lens, and finally refracted through the right surface of the lens. This product of matrices is written as follows

$$\mathcal{A} = R_2 T_{43} R_1 T_{32} T_{21} T_{10} \tag{3.1}$$

$$\mathcal{A} = \begin{bmatrix} 1 & -\left(\frac{n_a - n_3}{R_2}\right) \\ 0 & 1 \end{bmatrix} \begin{bmatrix} 1 & 0 \\ \frac{d_{43}}{n_3} & 1 \end{bmatrix} \begin{bmatrix} 1 & -\left(\frac{n_3 - n_a}{R_1}\right) \\ 0 & 1 \end{bmatrix} \begin{bmatrix} 1 & 0 \\ \frac{d_{32}}{n_a} & 1 \end{bmatrix} \begin{bmatrix} 1 & 0 \\ \frac{d_{21}}{n_1} & 1 \end{bmatrix} \begin{bmatrix} 1 & 0 \\ \frac{d_{10}}{n_a} & 1 \end{bmatrix}. \tag{3.2}$$

The index of refraction for air, the lenses, and the beam splitter are all predetermined values. $L1$ is a convex lens, so $R_1 = -R_2$. The distances d_{10}, d_{21}, d_{32} are all known or preset leaving d_{43} as the only unknown distance. $\mathcal{A}$ is then used to describe the ray transfer to this point

$$\overrightarrow{r_{t1}} = \mathcal{A}\overrightarrow{r_{i1}}. \tag{3.3}$$

Understanding the path of the beam to the point of the cantilever now allows for analysis of the beam from the cantilever to the PSD. As the beam reflects off the cantilever it diverges as it passes once again through the converging lens, $L1$ of Figure 20, which collimates the beam once again. This time as the beam passes through the beam splitter the percentage of the light being measured is sent horizontally to a second converging lens, $L2$, and into the PSD. The change in the deflection angle of the cantilever causes the movement of the beam spot on the PSD. This movement is characterized by $(\Delta x)L$ where x is the deflection angle and L is the total distance between the cantilever and the PSD.

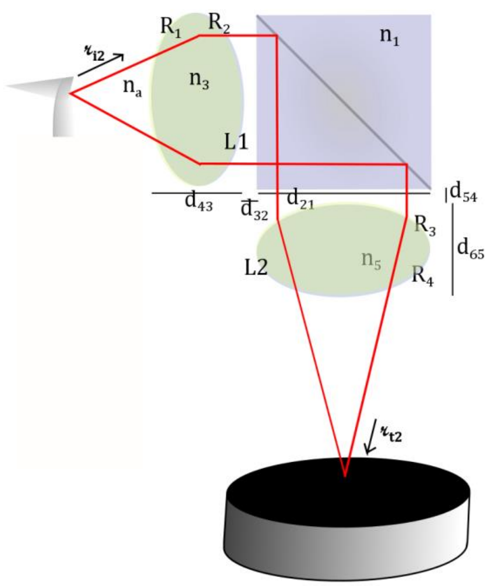

Figure 20. Drawing of the optics from the cantilever to the PSD. As the beam reflects off the cantilever, it diverges. The first converging lens will then collimate it. The beam splitter reflects the beam toward the second converging lens. This lens has a long focal length in order to provide a high resolution spot on the PSD.

A second matric system is used to analysis the setup from cantilever to PSD. The system matrix will determine the focal length of $L2$. The ray is now refracted through the left surface of $L1$, transmitted through the lens, and refracted through the right surface of the lens. It is then transmitted from the lens to the beam splitter and through the beam splitter. Finally it is refracted through the top surface of $L2$, transmitted through the lens, and refracted through the bottom surface of the lens.

This creates the lens matrix

$$\mathcal{A} = R_4 T_{65} R_3 T_{54} T_{21} T_{32} R_2 T_{43} R_1 \tag{3.4}$$

$$A = \begin{bmatrix} 1 & -\left(\frac{n_a - n_5}{R_4}\right) \\ 0 & 1 \end{bmatrix} \begin{bmatrix} 1 & 0 \\ \frac{d_{65}}{n_5} & 1 \end{bmatrix} \begin{bmatrix} 1 & -\left(\frac{n_5 - n_a}{R_3}\right) \\ 0 & 1 \end{bmatrix} \begin{bmatrix} 1 & 0 \\ \frac{d_{54}}{n_a} & 1 \end{bmatrix}$$
$$* \begin{bmatrix} 1 & 0 \\ \frac{d_{21}}{n_1} & 1 \end{bmatrix} \begin{bmatrix} 1 & 0 \\ \frac{d_{32}}{n_a} & 1 \end{bmatrix} \begin{bmatrix} 1 & -\left(\frac{n_a - n_3}{R_2}\right) \\ 0 & 1 \end{bmatrix} \begin{bmatrix} 1 & 0 \\ \frac{d_{43}}{n_3} & 1 \end{bmatrix} \begin{bmatrix} 1 & -\left(\frac{n_3 - n_a}{R_1}\right) \\ 0 & 1 \end{bmatrix}. \tag{3.5}$$

Again the indices of refraction are known. Similar to the first lens, $L2$ is a convex lens so $R_3 = -R_4$. The distance d_{43} was found in the previous system and d_{54} is set. Therefore, d_{65} is the only unknown distance. The final ray transfer is then

$$\overrightarrow{r_{t2}} = \mathcal{A}\overrightarrow{r_{\imath 2}}. \tag{3.6}$$

Having $\overrightarrow{r_{t2}}$ with respect to $\overrightarrow{r_{\imath 2}}$, allows the angle of deflection of the reflected beam due to the bending of the cantilever to be measured. The complete process is illustrated in Figure 16.

Chapter 4

CONCLUSION

4.1 Current Progress

Most of the designs for the AFM have been completed and need to be implemented. The optical laser system designs have been developed and are awaiting final analysis before the system can be assembled. As described in Section 3.4 a series of converging and diverging lenses will be needed in order to minimize the distance between the laser, the cantilever tip, and the PSD. Using refraction and transition matrices, a system of matrices has been created. This system can then be simplified to determine the correct thickness of each lens. The system of matrices needed to cover the distance from the laser to the cantilever and the path from the cantilever to the PSD have been designed. Once the optical laser system is assembled a new stage can be created to accommodate for the system. The control system for the Johnny Walker is nearing completion and will allow for data collection to begin once finished.

4.2 Future Plans

The two matrices that have been designed to represent the entire system need to be simplified and their results understood. This analysis will lead to the specifications needed for both the converging and diverging lenses needed in the system. Once all the specifications for the lenses are found the optical system can be put together.

The piezoelectric crystal on the cantilever holder has not been tested. Once the optical system is finalized the mount will need to be connected so that the cantilever can be driven to vibrate for imaging in tapping mode. The PSD will track the movement of the cantilever while the control system will move the walker. This change in movement provides an output that can be graphed to illustrate the topography of the sample.

The Johnny Walker will continue to be tested as movement of the legs has not been achieved yet. Once movement is seen and able to be reproduced it is also crucial that it is controlled. The walker must move walk up and down the ramps with a controlled and uniform movement such that the sample is approaching the cantilever as needed.

Once the cantilever is oscillating, the PSD is able to collect the necessary data, and the walker movement has been defined the final steps in assembling the AFM can begin. In order to accommodate for the new designs the isolation stage will need to be rebuilt. Once the AFM has been assembled data collection can begin.

4.3 Conclusion

The completion of the Atomic Force Microscope will allow the Houghton College Physics Department to further their research of thin metal films. When operable it will be able to provide topological images with nanometer resolution of the scanned samples. In addition to research goals the AFM has many educational goals. The necessary design and construction work needed to make the AFM operable has created and will continue to create many opportunities to expand students understanding in construction, electronics, problem solving, optics, and other important skills.

[1] G. Binning, C.F. Quate, and Ch. Gerber, Phys. Rev. Lett., **56** (9), 930 (1986).

[2] A.J.M Wollman et al, Open Biol., (2015).

[3] E. Ruska, Nobel Lecture, (Berlin, 1986).

[4] FEI Company, *An Introduction to Electron Micrsocopy, (*Hillsboro*, OR,* 2010).

[5] D. Rugar and P. Hansma, Phys. Today **3** (10), 23 (1990).

[6] G. Binnig et al, Phys. Rev. Lett., **49** (1), 57 (1982)

[7] G. Binnig, H.*U.S. Patent No. 4,724,318*. Washington, DC: U.S. Patent and Trademark Office, (1988).

[8] N. Amer and G. Meyer, *U.S. Patent No. 5,144,833*. Washington, DC: U.S. Patent and Trademark Office, (1992).

[9] L.B. Freund and S. Suresh, *Thin Film Materials: Stress, Defect Formation, and Surface Evolution* (University Press, Cambridge, 2003), p. 3.

[10] T. Yoshitake et al., Appl Surf. Sci., **141**, 129-137 (1999).

[11] AFM Workshop, *Price List,* http://www.afmworkshop.com/atomic-force-microscope-prices.html, (3 Nov 2016).

[12] M. Nasehnejad, M. Shahraki, G. Nabiyouni, Appl. Surf. Sci., **389**, 735-741 (2016).

[13] Y. Martin, C.C. Williams, and H.K. Wickramasinghe, J. Appl. Phys., **61** (10), 4723 (1987).

[14] H.C. Hamaker, Physica, **IV** (10), 1058-1072 (1937).

[15] J. Hutter and J. Bechhoefer, J. Appl. Phys., **73** (9), 4123-4129 (1993).

[16] S. Magonov and N. Yerina. *Microscopy for Nanotechnology* (Springer, 2005), p. 113-155.

[17] E. Ocock, B.S. Thesis, Houghton College, 2014.

[18] Physik Instrumente, *PT Piezo Scanner Tubes*, http://www.physikinstrumente.com, (2014).

[19] O. Svelto, *Principles of Lasers* (Springer, 2010), p. 131-161.

[20] B. Little, B.S. Thesis, Houghton College, 2009.

[21] J. Yuly, B.S. Thesis, Houghton College, 2016.

[22] *Position Sensing Detector CONEX-PSD Series,* (Newport, Irvine, 2015).